IEEE Access
Multidisciplinary ⋮ Rapid Review ⋮ Open Access Journal

Received November 4, 2020, accepted November 16, 2020, date of publication November 20, 2020,
date of current version December 10, 2020.

Digital Object Identifier 10.1109/ACCESS.2020.3039546

An Online Adaptive Control Strategy for Trajectory Tracking of Quadrotors Based on Fuzzy Approximation and Robust Sliding Mode Algorithm

BOWEN XU AND XINJIANG LU, (Member, IEEE)
State Key Laboratory of High Performance Complex Manufacturing, Central South University, Changsha 410082, China

Corresponding author: Xinjiang Lu (luxj@csu.edu.cn)

This work was supported in part by the National Natural Science Foundation of China under Grant 51675539, and in part by the Hunan Provincial Natural Science Foundation of China under Grant 2019JJ20030.

ABSTRACT In this paper, an online adaptive control strategy is proposed for the accurate trajectory tracking of quadrotor unmanned aerial vehicles (UAVs) under time-varying model uncertainties and external disturbances. A robust sliding mode controller was developed for the outer-loop position subsystem to guarantee robust tracking performance even under disturbance. For the inner-loop attitude subsystem, an online adaptive controller was designed, which integrated the fuzzy and SMC into one unified system. Critically, its parameters were simultaneously identified and adjusted in real-time. These sub-control systems were then integrated into a unified closed-loop system. Its uniform stability was then analyzed and strictly proofed. Case studies demonstrated the effectiveness of our proposed strategy, along with its superior control performance when compared with several commonly used methods.

INDEX TERMS Quadrotor UAVs, nonlinear control, fuzzy system, sliding mode control, trajectory tracking.

I. INTRODUCTION

Recently, quadrotor unmanned aerial vehicles (UAVs) have seen increased and extensive use across various areas, including the military, agriculture, search and rescue, fire-fighting, environmental protection, and personal entertainment. The popularity of UAVs has been due to their security and maneuverability. Compared with helicopters and fixed-wings UAVs, the quadrotor possesses many significant advantages, such as vertical take-off and landing capacities, strong maneuverability, simple mechanical structure, and low cost. Moreover, the flexible design performance of both its size and specification allows quadrotors to be rapidly adapted to the requirements of a given industry [1], [2]. Despite these benefits, the desirable trajectory tracking performance of the quadrotor is always affected by uncertain internal and external nonlinearities in the actual flight environment. It is difficult to obtain an accurate model of the system, since the quadrotor is a typical dynamic nonlinear system with strongly coupled and underactuated characteristics, along with unexpected model uncertainties caused by airframe vibration and air resistance. Furthermore, wind gusts and payload variation usually lead to multi-frequency disturbances and chattering during the actual flight, all of which influence tracking accuracy and flight stability of the quadrotor. This is especially true for the electromechanical actuators. With these problems in mind, it has become greatly important to design an efficient controller with satisfactory trajectory-tracking accuracy and robust performance for quadrotors under such model uncertainties and external disturbances [3]–[6].

With regard to these problems, significant amount of research has been devoted to achieving better performance for the trajectory tracking of quadrotors. Different strategies have been proposed, including proportional-integral-derivative (PID), the backstepping method, sliding mode control, fuzzy algorithm, and the adaptive control method [7]–[12].

Initially, linear control algorithms such as single loop or multi-loop PID and linear quadratic regulator (LQR) were widely applied to control the quadrotor. This was because they had advantages in both simplicity and practicability [13], [14]. These algorithms performed reasonably well when the aircraft worked in actual operating conditions. For

The associate editor coordinating the review of this manuscript and approving it for publication was Jinquan Xu.

This work is licensed under a Creative Commons Attribution 4.0 License. For more information, see https://creativecommons.org/licenses/by/4.0/

instance, a PID cascade control of the quadrotor for trajectory tracking with small acceleration was proposed in [14]; its tracking performance was shown to be excellent for low velocities. However, the fitting effect and control accuracy of these algorithms for nonlinearities were unsatisfactory. This was mainly because many of the controllers proposed in these previous studies were based on models and required almost a full knowledge of its dynamics. In turn, this led to a heavy dependence on the model's accuracy. Additional work sought to address this limitation by using an increasing number of nonlinear control methods in quadrotors, which were somewhat effective [15].

As a commonly used nonlinear algorithm, the backstepping algorithm allows for online control performance by using a reverse design method [10], [11]. However, the strict requirement on the model's structure remains a large restriction for this algorithm. Due to its outstanding properties of fast responsivity, disturbance insensitivity, and independent features in the model's structure [16], many researchers have concentrated their studies on using and introducing the sliding mode control (SMC) into quadrotor control. By designing different sliding equations, the SMC converges to a uniform, asymptotical stability at exponential speed. Importantly, this approach has been effective in trajectory tracking and random disturbance response [9], [17]–[19]. In [17], a robust second order sliding mode controller (SOSM) was proposed with good transient performance on the altitude tracking of the quadrotor. When combined with the SMC, the limitations of the backstepping method were overcome. In [9], a backstepping sliding mode controller (Integral BS-SMC) was designed to improve the system's robustness against external disturbances. However, there were still several defects in the actual application of the SMC, including convergence time, the robust term, and high frequency chattering [20]–[23]. Several solutions, such as super twisting algorithm (STA) [24], have been proposed to address such defects [25]–[27], and strong robustness was introduced to overcome both internal and external parametric perturbations. In [24], STA was applied to a quadrotor to ensure robustness against bounded disturbances and its finite time convergence was proved by means of a majorant curve. Two different kinds of two-sliding mode control algorithms were proposed in [26] by bounding the model dynamics with positive functions. This approach led to a reduction in the chattering effect. However, the STA had some shortcomings related to the strength of disturbances. For instance, the traditional linear STA cannot deal with strong disturbance near the origin, while the nonlinear STA is not able to endure a linearly growing perturbation the introduction of discontinuous. Besides, the introduction of robust terms also triggered high-frequency dynamic system errors, which was extremely dangerous for the electromechanical actuators.

Since the built-in gyroscope of the quadrotor is highly sensitive to the attitude acceleration variable of the airframe, real-time calculations are often necessary to overcome the system dynamics and environmental changes. In this context, an increasing number of intelligent control strategies have attracted considerable research interest and have been introduced into the trajectory tracking system of the quadrotor [18], [28], [29], [39], [40]. This is especially true for hybrid controllers combined with fuzzy control algorithm. By introducing human experience into the controlling process, these intelligent algorithms guarantee an accurate approximation to the model's uncertainties [30]–[34]. When combined with an adaptive strategy, the intelligent control system allowed for real-time regulation of system parameters according to its actual state [35]–[37]. In [18], an adaptive fuzzy gain-scheduling sliding mode control (AFGS-SMC) was proposed for unmanned quadrotors; this was done to regulate attitude parametric uncertainties. In [31], a hierarchical control strategy was proposed for positional and attitude tracing of quadrotors. This approach was based on the double-loop integral sliding mode control (IntSMC) along with the adaptive radical basis function neural networks (RBFNNs). In [37], a nonlinear adaptive controller was proposed for orientation and translation tracking of the quadrotor using the adaptive nonsingular fast terminal SMC (ANFT-SMC).

Despite these advances, there remain several limitations in these past works: (1) A consideration of system-wide perspective is lacked, and only parts of the control loop were studied, i.e., the altitude subsystem or the attitude subsystem. (2) There are few studies on considering both internal uncertainty and external disturbances. (3) When time-varying and nonlinear dynamics of the system is very strong, only using online modeling or online control is often difficult to achieve a satisfactory performance.

Aiming to these challenges, in combination with the advantages of both adaptive fuzzy control and a robust second order sliding mode algorithm, we propose a novel online adaptive control strategy for quadrotor UAVs in trajectory tracking against dynamic model uncertainties and external disturbances. The virtual variable method was used to effectively decouple the relationship between the inner-loop attitude control and the outer-loop position control. Detailed contributions of this paper are highlighted as follows:

- Based on the first-order tracking error, a robust sliding mode controller was proposed for the outer-loop position subsystem to alleviate external disturbances and guarantee robust tracking performance.
- An adaptive nonlinear sliding mode controller was designed for the attitude subsystems by integrating the fuzzy system and robust sliding mode control into a unified framework, in which the parameters were simultaneously identified and adjusted in real-time.
- These sub-control systems were then integrated into a unified closed-loop system and the uniform stability of overall system was theoretical analyzed and strictly proved.
- Case studies demonstrated the effectiveness of our proposed strategy, along with its superior control performance when compared with several commonly used methods.

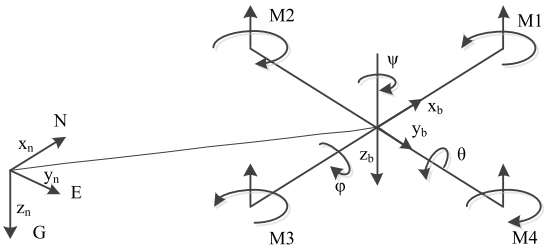

FIGURE 1. Coordinate systems for quadrotor UAVs.

The rest of this paper is organized as follows: Section 2 presents the dynamic model of the quadrotor and the control problem existing in the quadrotor UAVs. Section 3 proposes the online adaptive control strategy, while Section 4 describes the use of several comparison and trajectory tracking simulations to verify the effectiveness and robustness of the elaborated control strategy.

II. MODELING AND PROBLEM DESCRIPTION

Assumed that the quadrotor UAV is rigid, and the centroid of mass is concentrated in the geometric center. As shown in Fig.1, the body-frame coordinate system and the geographic coordinate system are defined for the modeling process. The body-frame coordinate system (b system) is affixed and connected with the centroid, while the coordinate system rotates following the rotation of the quadrotor. In the geographic coordinate system, i.e. the inertial/ navigation coordinate system (named n system), the x-axis refers to the North (N), the y-axis to the East (E), and the z-axis to the earth (G). Suppose that θ, φ, ψ represent the pitch, roll, and yaw angles in the body-frame coordinate, respectively, and x, y, z represent the position of the centroid in the inertial coordinate system.

According to Newton mechanics and the Newton-Lagrange equation, dynamic equations of the quadrotor with respect to the inertial coordinates can be generally expressed as [4]–[6], [12]

$$\begin{cases} \ddot{\phi} = \dfrac{I_y - I_z}{I_x}\dot{\theta}\dot{\psi} + \dfrac{1}{I_x}U_2 + \dfrac{I_r}{I_x}\dot{\theta}\omega_{sum} - \dfrac{K_1 l}{I_x}\dot{\phi} \\ \ddot{\theta} = \dfrac{I_z - I_x}{I_y}\dot{\phi}\dot{\psi} + \dfrac{1}{I_y}U_3 - \dfrac{I_r}{I_y}\dot{\phi}\omega_{sum} - \dfrac{K_2 l}{I_y}\dot{\theta} \\ \ddot{\psi} = \dfrac{I_x - I_y}{I_z}\dot{\phi}\dot{\theta} + \dfrac{1}{I_z}U_4 - \dfrac{K_3 l}{I_z}\dot{\psi} \\ \ddot{x} = \dfrac{U_1}{m}\left(cos\phi sin\theta cos\psi + sin\phi sin\psi\right) - \dfrac{1}{m}K_{\mathrm{ax}}\dot{x} \\ \ddot{y} = \dfrac{U_1}{m}\left(cos\phi sin\theta sin\psi - sin\phi cos\psi\right) - \dfrac{1}{m}K_{\mathrm{ay}}\dot{y} \\ \ddot{z} = \dfrac{U_1}{m}cos\phi cos\theta - g - \dfrac{1}{m}K_{\mathrm{az}}\dot{z} \end{cases} \tag{2-1}$$

where l represents the distance from centroid to propeller shaft, $\omega_{sum} = -\omega_1 + \omega_2 - \omega_3 + \omega_4$, d is the resistance coefficient, b is the lifting coefficient, $\omega_i (i = 1, 2, 3, 4)$ represents the angular velocity of each propeller, I_r is the inertial moment of propeller. I_x, I_y, I_z are the moment of inertia. g denotes the acceleration of gravity, $K_{\mathrm{ax}}, K_{\mathrm{ay}}, K_{\mathrm{az}}$ represent the rotation resistance coefficient matrix of each propeller. $\dot{x}$, $\dot{y}$, $\dot{z}$ are the translational velocity of the quadrotor in the inertial coordinate system. U_1 represents the control input of four independent control channels (altitude, roll, pitch, and yaw).

In the actual flight, the lift of the quadrotor is mainly produced by the rotation of propellers. Firstly, according to the gravity of the aircraft, the rotation speed of each propeller is obtained by reverse calculation, so that the aircraft obtains the basic lift through four propellers to offset its own gravity. Then, based on the basic thrust, the controller mainly focuses on the incremental and decremental adjustment, which means that speed of four motors is adjusted according to the deviation between the target point and current position.

As shown in Eq. (2-1), the rotational information $\ddot{\phi}$, $\ddot{\theta}$, $\ddot{\psi}$ is related to U_2, U_3, U_4, respectively; similarly, the position acceleration $\ddot{x}$, $\ddot{y}$, $\ddot{z}$ is related to U_1, m, ϕ, ψ, θ. The following practical problems may result in the model and control difficulties: (1) different forms of wind gusts in the actual flight environment, i.e., abrupt, high-frequency, whirlwind etc., which will influence the robustness of the controller; (2) the airframe vibration caused by external factors such as air resistance, which may result in model uncertainties.

As the control loops shown in Fig. 2, when tracking the target trajectory, the outer-loop position controller will call the corresponding algorithm based on the input target trajectory and the real position information to control the quadrotor's angle. This transfers the output regular velocity deviation to the inner-loop attitude controller. The inner-loop then adjusts the attitude of the aircraft according to this deviation, after which it transfers the thrust information to the final executive units.

A. POSITION SUBSYSTEM

According to reference [34], the following two virtual variables U_x and U_y are introduced to decouple the relationship between the inner- and outer-loop control systems.

$$\begin{cases} U_x = U_1(cos\phi sin\theta cos\psi + sin\phi sin\psi) \\ U_y = U_1(cos\phi sin\theta sin\psi - sin\phi cos\psi) \\ U_z = U_1 cos\phi cos\theta \end{cases} \tag{2-2}$$

Then we have

$$\theta = arctan\left((U_x cos\psi + U_y sin\psi)/U_z\right) \tag{2-3}$$

$$\Phi = arctan(\left(cos\theta(U_x sin\psi - U_y cos\psi)/U_z\right)) \tag{2-4}$$

Suppose that the model uncertainties in x, y, z dimensions are [23] $\chi_1(t, x, \dot{x})$, $\chi_2(t, y, \dot{y})$, $\chi_3(t, z, \dot{z})$. There are many random uncertainties in actual flight environment, and the prior empirical knowledge is difficult to obtain in real-time. The typical example is wind gusts, which has high-frequency or multi-frequency characteristics [4]. Here we suppose that $\gamma(t) = [\gamma_1(t), \gamma_2(t), \gamma_3(t)]$ denotes the external disturbances caused by external disturbances in x,

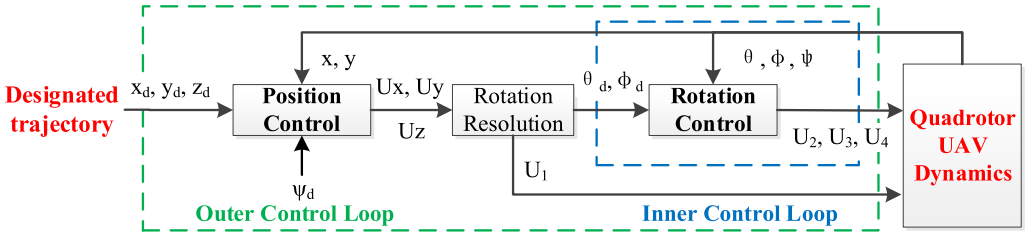

FIGURE 2. Overall control loop structure of quadrotor UAVs.

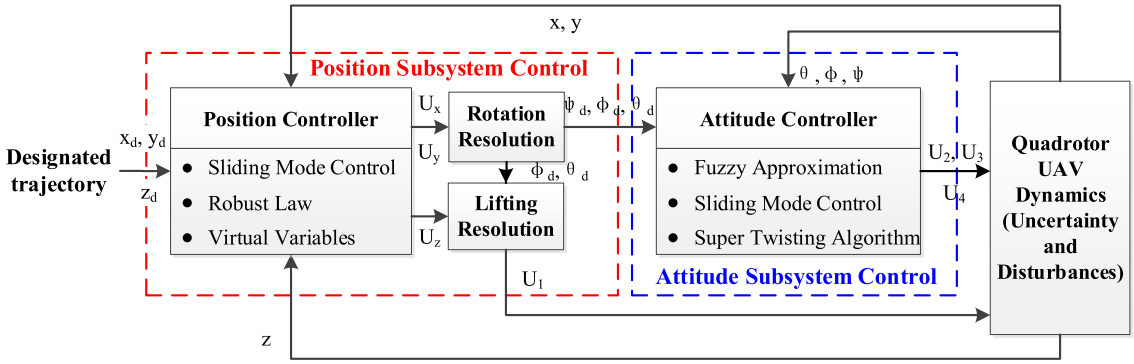

FIGURE 3. The entire framework of the elaborated control strategy for quadrotor UAV.

y, z directions. The state variables in position x, y, z can be rewritten as

$$\begin{cases} m\ddot{x} = U_x - K_{ax}\dot{x} + \chi_1(t, x, \dot{x}) + \gamma_1(t) \\ m\ddot{y} = U_y - K_{ay}\dot{y} + \chi_2(t, y, \dot{y}) + \gamma_2(t) \\ m\ddot{z} = U_z - K_{az}\dot{z} - mg + \chi_3(t, z, \dot{z}) + \gamma_3(t) \end{cases} \tag{2-5}$$

In the outer-loop translation altitude subsystems and with the predefined target position (x_d, y_d, z_d), the virtual control variables U_x, U_y and U_z are calculated by Eq. (2-5). Then we can get the attitude angles ϕ, θ and U_1 directly through Eqs. (2-2), (2-3) and (2-5), which are regarded as the target angles of the inner-loop attitude subsystem.

B. ATTITUDE SUBSYSTEM

According to the dynamic attitude expression in Eq. (2-1), the attitude equation can be expressed as [28], [41]

$$D\ddot{q}(t) = f(t, q, \dot{q}) + U(t) + \tau(t) \tag{2-6}$$

$$f(t, q, \dot{q}) = C(\dot{q})\dot{q} + \xi(t, q, \dot{q}) \tag{2-7}$$

where $q = (\phi, \theta, \psi)^T$.$\tau(t)$ is a 3×1 dimensional matrix, and represents the disturbance to the built-in gyroscope. D, $C(\dot{q})$, $U(t)$ represent

$$D = \begin{bmatrix} I_x & 0 & 0 \\ 0 & I_y & 0 \\ 0 & 0 & I_z \end{bmatrix}, \quad U(t) = \begin{bmatrix} U_2 \\ U_3 \\ U_4 \end{bmatrix}$$

$$C(\dot{q}) = \begin{bmatrix} 0 & 0 & (I_y - I_z)\dot{\theta} \\ (I_z - I_x)\dot{\psi} & 0 & 0 \\ 0 & (I_x - I_y)\dot{\phi} & 0 \end{bmatrix}$$

$\xi(t, q, \dot{q})$ denote nonlinear model uncertainties, including the vibration and the ignorance structure of the airframe, which is inspired by the following two parts: (1) In actual flight, the air resistance of the propellers is almost basically in direct proportion to square of rotor speed [28]. (2) In the modeling process, the rotation resistance terms (e.g., $I_r\dot{\theta}\omega_{sum}/I_x, I_r\dot{\phi}\omega_{sum}/I_y$) of attitude subsystem is always ignored to simplify the subsystem during the modelling process, which influences the modeling accuracy and even results in severe distortion to physical devices.

III. CONTROL DESIGN

To address the problem described above, we propose a combinatorial, nonlinear control strategy for trajectory tracking in quadrotors when dealing with dynamic model uncertainties and external disturbances. As shown in Fig. 3, for the outer-loop position subsystem, a robust sliding mode controller was established to realize the horizontal position, in which the integration of first-order tracking error was introduced to enhance the robustness against external disturbances. For the inner-loop attitude subsystem, an adaptive fuzzy sliding mode controller was designed in combination with both the fuzzy algorithm and SMC, in which an improved STA was designed to guarantee the robustness of the system to external disturbances. These sub-control systems were then integrated into a unified closed-loop system.

Moreover, according to Fig.3, when carrying out control of the position subsystem, the chattering caused by control switching of attitude subsystem can be regarded as external disturbance, and the integration of first-order tracking error was introduced to enhance the robustness against external

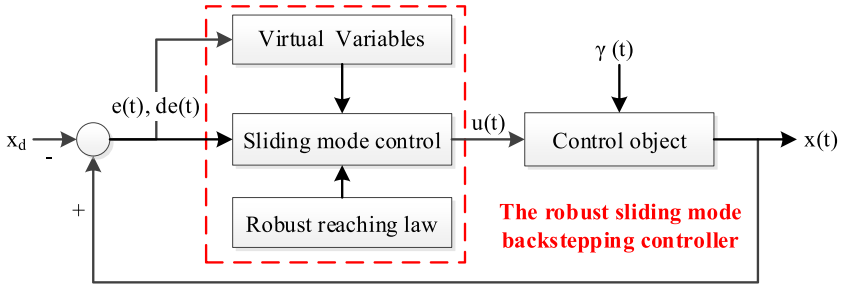

FIGURE 4. Proposed structure of the robust sliding mode controller.

disturbances. When carrying out control of the attitude, the chattering caused by control switching of position subsystem is also regarded as external disturbance, and the fuzzy and super twisting algorithm were introduced to guarantee the robustness to disturbance. In this way, the chattering caused by control switching is suppressed.

A. POSITION CONTROLLER DESIGN

As described in (2-5), by introducing three virtual variables U_x, U_y and U_z, the translational movement equations can be simplified as [25]

$$m\ddot{x} = U_x - K_{ax}\dot{x} + \delta_1(t, x, \dot{x}) \tag{3-1}$$
$$m\ddot{y} = U_y - K_{ay}\dot{y} + \delta_2(t, y, \dot{y}) \tag{3-2}$$
$$m\ddot{z} = U_z - K_{az}\dot{z} - mg + \delta_3(t, z, \dot{z}) \tag{3-3}$$

where $\delta_1(t, x, \dot{x}) = \chi_1(t, x, \dot{x}) + \gamma_1(t)$, $\delta_2(t, y, \dot{y}) = \chi_2(t, y, \dot{y}) + \gamma_2(t)$, $\delta_3(t, z, \dot{z}) = \chi_3(t, z, \dot{z}) + \gamma_3(t)$.

Although the model uncertainties and disturbances are unpredictable in actual flight and could not be known as a prior, the effects of those factors can be alleviated by the proposed control item. Therefore, a robust sliding mode controller was constructed to realize the accurate and stable movement in three dimensions, which is shown in Fig. 4.

Here, we take the x direction as an example to illustrate the controller design process. In this controller, virtual variables are designed to ensure that the system is asymptotically bounded, so the control output not only suppresses disturbances, but also realizes the asymptotic tracking on reference signals.

By defining two state variables x_1, x_2, Eq. (3-1) can be rewritten as the following state-space form:

$$\begin{cases} \dot{x}_1 = x_2 \\ \dot{x}_2 = \dfrac{1}{m}U_x - \dfrac{K_{\text{ax}}}{m}x_2 + \dfrac{1}{m}\delta_1(t, x_1, x_2) \end{cases} \tag{3-4}$$

where $U_x = U_1(cos\phi sin\theta cos\psi + sin\phi sin\psi)$; x_1, x_2 represent velocity and acceleration in x-direction respectively, which are used to describe the system's motion state in x direction.

Inspired by the backstepping technique, we introduce the virtual variable β and the first-order tracking error $\int_0^t e_{1x}(\tau)d\tau$, to ensure the tracking robustness.

$$\beta = \dot{x}_{1d} - J_0\int_0^t e_{1x}(\tau)d\tau - J_1 e_{1x}, J_0, J_1 > 0 \tag{3-5}$$

Define two error variables e_{1x}, e_{2x} and set

$$\begin{cases} e_{1x} = x_1 - x_{1d} \\ e_{2x} = x_2 - \beta \end{cases} \tag{3-6}$$

Then we have the sliding surface:

$$s_x = c_x e_{1x} + e_{2x} \tag{3-7}$$

where c_x is the convergence parameter.

Moreover, from Eq. (3-6)

$$\dot{e}_{2x} = \frac{1}{m}U_x - \frac{K_{\text{ax}}}{m}x_2 + \frac{1}{m}\delta_1(t, x_1, x_2) - \ddot{x}_{1d} + J_1\dot{e}_{1x} + J_0 e_{1x} \tag{3-8}$$

where $J_0, J_1 > 0$. Define the following exponential approach law to improve the robustness of the translational control system

$$\dot{s}_x = -\rho_1 sign(s_x) - \rho_2 s_x, \quad \text{where } \rho_1, \rho_2 > 0 \tag{3-9}$$

Define the Lyapunov function

$$V = \frac{1}{2}s_x^2 \tag{3-10}$$

and set the robust control law:

$$U_x = K_{\text{ax}}x_2 + m\left(\ddot{x}_{1d} + c_x\left(J_1 e_{1x} + J_0\int_0^t e_{1x}(\tau)\,d\tau - e_{2x}\right) - (J_1\dot{e}_{1x} + J_0 e_{1x} + \rho_1 sign(s_x) + \rho_2 s_x)\right) \tag{3-11}$$

Then the differential of Eq. (3-10) is

$$\begin{aligned} \dot{V} &= s_x\dot{s}_x = s_x(c_x\dot{e}_{1x} + \dot{e}_{2x}) \\ &= s_x\left[c_x(x_2 - \dot{x}_{1d}) + \frac{1}{m}U_x - \frac{K_{\text{ax}}}{m}x_2 + \frac{1}{m}\delta_1(t, x_1, x_2) - \ddot{x}_{1d} + J_1\dot{e}_1 + J_0 e_1\right] \\ &= -\rho_1|s_x| - \rho_2 s_x^2 + \frac{s_x}{m}\delta_1(t, x_1, x_2) \\ &\le -\rho_2 s_x^2 - |s_x|(\rho_1 - \frac{\delta_1^u}{m}) \end{aligned} \tag{3-12}$$

where δ_1^u is the upper bound of disturbance $\delta_1(t, x_1, x_2)$.

Clearly, when $\rho_1 > \frac{\delta_1^u}{m}$, $\rho_2 > 0$, $\dot{V} < 0$, the sliding surface $s \to 0$ and the translation subsystem is asymptotically stable.

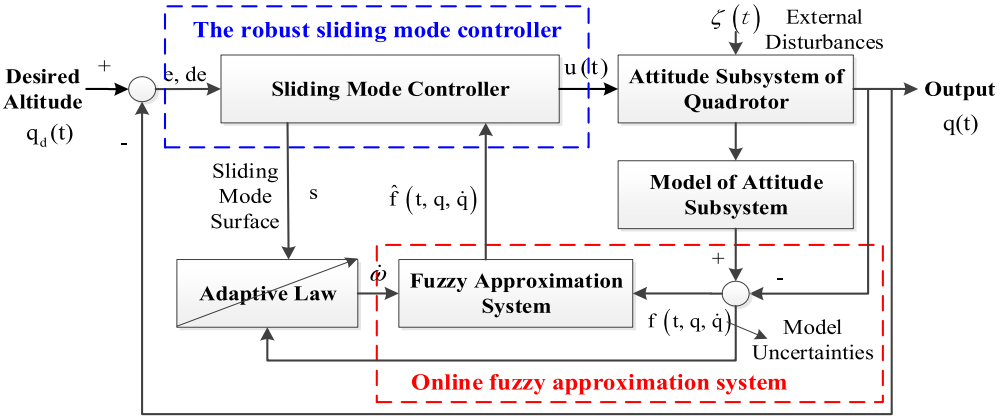

FIGURE 5. Proposed attitude control structure based on fuzzy adaptive sliding mode algorithm.

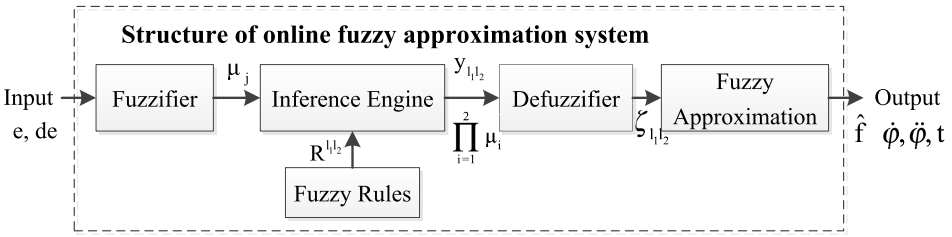

FIGURE 6. Structure of the proposed online fuzzy approximation system.

Similarly, control inputs in y and z directions can be obtained and expressed as

$$U_y = K_{ay}y_2 + m(\ddot{y}_{1d} + c_y(J_3e_{1y} + J_2\int_0^t e_{1y}(\tau)\,d\tau - e_{2y}) - (J_3\dot{e}_{1y} + J_2e_{1y}) - \rho_3 sign(s_y) + \rho_4 s_y) \quad (3\text{-}13)$$

$$U_z = K_{az}z_2 + m(\ddot{z}_{1d} + c_y(J_5e_{1y} + J_4\int_0^t e_{1z}(\tau)\,d\tau - e_{2z}) - (J_5\dot{e}_{1z} + J_4e_{1z}) - \rho_5 sign(s_z) + \rho_6 s_z) + mg \quad (3\text{-}14)$$

B. ATTITUDE CONTROLLER DESIGN

For the attitude sub-control system, an online adaptive fuzzy sliding mode controller was elaborated for attitude tracking accuracy. As shown in Fig. 5, this method uses both the fuzzy model and SMC to overcome uncertainties and external disturbances, respectively. Moreover, to alleviate the chattering problem existing in the traditional SMC, we introduced an improved STA, in which the chattering switch function is applied to higher-order derivative of the sliding mode variable by introducing the integral term and the exponential term. On this basis, an online adaptive strategy was also designed to integrate the fuzzy model and robust SMC into a unified framework, so that the parameters of the control system would be simultaneously identified in real-time.

Due to the simplicity and practicability in modeling, it is difficult to obtain an accurate equation of $f(t, q, \dot{q})$. According to the universal approximation theorem [32], there must be a fuzzy system $\hat{f}(t, q, \dot{q})$ highly approximate to $f(t, q, \dot{q})$; in this way, it is reasonable to use $\hat{f}(t, q, \dot{q})$ constructed on the two-dimensional fuzzy controller to approximate $f(t, q, \dot{q})$. Here and to ensure approximation accuracy, ε is defined as the approximation error.

From Eq. (2-6), we know that there are three angle variables in the attitude control system, and all should be considered when designing the fuzzy system. Here, we use pitch angle ϕ as an example. The detailed fuzzy approximation processes are shown in Fig. 6.

Assume that A_1 and A_2 represent the fuzzy sets of φ_1 and φ_2 respectively, B denotes the result set. $l_1 = 1, 2, \cdots, m; l_2 = 1, 2, \cdots, n$ is the elements number of each fuzzy set. $A_1^{l_1}$ and $A_2^{l_2}$ are the element fuzzy sets of A_1 and A_2, m and n represent the element number of $A_1^{l_1}$ and $A_2^{l_2}$. $B_{l_1l_2}$ is the fuzzy result. Then the fuzzy rules can be built as follows:

$$R^{(l_1l_2)}: IF\ \varphi_1\ is\ A_1^{l_1}\ and\ \varphi_2\ is\ A_2^{l_2}\ THEN\ \hat{f}\ (\phi\,|\,\omega_\phi)\ is\ B_{l_1l_2}$$

Currently, there are several studies on fuzzy systems with trigonometric [12] and Gaussian functions [18], [30], in which the satisfactory approximation performance for uncertain disturbances has been demonstrated, especially the Gaussian function. Here the membership function is selected as:

$$\mu_j = exp\left(-\frac{\|\phi - c_j\|^2}{2b_j^2}\right), \quad j \in \{l_1, l_2\} \quad (3\text{-}15)$$

In the fuzzy system, the singleton fuzzifier is used to calculate the rule result and the function value $y_{l_1l_2}$ corresponds

TABLE 1. Description of the fuzzy calculation procedures.

Input: l_1, l_2, m, n;
ϕ_d: the target pitch angle; ϕ: the real-time pitch angle;
$e_\phi = \phi_d - \phi$, $\dot{e}_\phi = \dot{\phi}_d - \dot{\phi}$
Fuzzy sets φ_1 and φ_2; % singleton fuzzifier sets of e_ϕ and $\dot{e}_\phi$
Repeat % closed control loop
1. Define two $l_1 * l_2$Matrix FS and $\zeta(\phi)$;
2. Initiating YFS and TFS to 0;
3. for $l_1 = 1,2,\cdots,m$ do % elements number of fuzzy sets φ_1
4. for $l_2 = 1,2,\cdots,n$ do % elements number of fuzzy sets φ_2
5. $FS[l_1 l_2] = \prod_{i=1}^{2} \mu_{l_i}(\varphi_i)$ % result of each product inference engine
6. $YFS+= y_{l_1 l_2}(FS(l_1 l_2))$ % summation of function values $y_{l_1 l_2}$
7. $TFS+= (FS(l_1 l_2))$
8. endfor
9. endfor
10. $\hat{f}(\phi|\omega_\phi) = YFS/TFS$ % fuzzy results based on center average method
11. $\zeta(\phi) = FS/(TFS + 0.001)$ % output of the defuzzifier
Output $\zeta(\phi)$

to the maximum value of the membership function. Moreover, implying the product inference machine, the inference conclusions can be formulated as $y_{l_1 l_2} \prod_{i=1}^{2} \mu^{l_i}(\varphi_i)$. Thus, the system output is obtained based on the center average defuzzifier

$$\hat{f}(\phi \mid \omega) = \frac{\sum_{l_1=1}^{m} \sum_{l_2=1}^{n} y_{l_1 l_2} \left(\prod_{i=1}^{2} \mu^{l_i}(\varphi_i) \right)}{\sum_{l_1=1}^{m} \sum_{l_2=1}^{n} \left(\prod_{i=1}^{2} \mu^{l_i}(\varphi_i) \right)} \quad (3\text{-}16)$$

where $\mu^{l_i}(\cdot)$ represents the membership function.

Define parameter ω_ϕ and introduce a new $\zeta(\phi) \in \mathbb{R}^{m \times n}$, then we have the fuzzy output

$$\hat{f}(\phi \mid \omega_\phi) = \hat{\omega}_\phi^T \zeta(\phi) \quad (3\text{-}17)$$

Then the $\zeta(\phi)$ for $l_1 l_2 th(l_1 = 1, 2, \cdots, m; l_2 = 1, 2, \cdots, n)$ members can be expressed as:

$$\zeta_{l_1 l_2}(\phi) = \frac{\prod_{i=1}^{2} \mu^{l_i}(\varphi_i)}{\sum_{l_1=1}^{m} \sum_{l_2=1}^{n} \left(\prod_{i=1}^{2} \mu^{l_i}(\varphi_i) \right)} \quad (3\text{-}18)$$

The description of the fuzzy calculation procedures is shown in Table 1.

Assuming that

$$\omega_\phi^* = arg \min_{\omega \in \Omega} \left[\sup_{\phi \in \Omega} \left| \hat{f}(\phi \mid \omega) - f(\phi) \right| \right] \quad (3\text{-}19)$$

then we have

$$f(\phi) = \omega_\phi^{*T} \zeta(\phi) + \varepsilon \quad (3\text{-}20)$$

where ε represents the approximation error.

Defining $\tilde{\omega}_\phi^T = \hat{\omega}_\phi^T - \omega_\phi^{*T}$, then

$$\begin{aligned} f(\phi) - \hat{f}(\phi \mid \omega) &= \omega_\phi^{*T} \zeta(\phi) + \varepsilon - \hat{\omega}_\phi^T \zeta(\phi) \\ &= -\tilde{\omega}_\phi^T \zeta(\phi) + \varepsilon \end{aligned}$$

Similarly, with $W_q = [\omega_\phi, \omega_\theta, \omega_\psi]^T$ we have

$$\hat{f}(t, q, \dot{q}) = W_q^{*T} \zeta(q, t) + E$$

and the dynamic attitude equation can be rewritten as

$$D\ddot{q}(t) = f(t, q, \dot{q}) + U(t) + \tau(t) \quad (3\text{-}21)$$

$$\begin{aligned} \tilde{f}(t, q, \dot{q}) &= f(t, q, \dot{q}) - \hat{f}(t, q, \dot{q}) \\ &= -\tilde{W}_q^T \zeta(q, t) + E \end{aligned} \quad (3\text{-}22)$$

where $D = \begin{bmatrix} I_x & 0 & 0 \\ 0 & I_y & 0 \\ 0 & 0 & I_z \end{bmatrix}$, $U = \begin{bmatrix} U_2 \\ U_3 \\ U_4 \end{bmatrix}$. I_x, I_y, I_z represent the moment of inertia. $\tilde{W}_q^T = \hat{W}_q^T - W_q^{*\mathrm{T}}$, $E = [\varepsilon_1, \varepsilon_2, \varepsilon_3]^T$. $\varepsilon_1, \varepsilon_2, \varepsilon_3$ are the approximation error of θ, φ, ψ respectively.

With the former proposed fuzzy approximation system, model uncertainties of the system can be compensated. To obtain better satisfactory tracking accuracy and robust performance against external disturbances, an adaptive robust controller was further elaborated. In this controller, an improved STA was introduced as the robust term to alleviate the chattering problem existing in the traditional sliding mode controller. The robust approaching law varied according to the real-time feedback state and fuzzy approximation term. The structure of the robust sliding mode algorithm is shown in Fig. 7.

Define the sliding mode function

$$s_q = \lambda e + \dot{e} \quad (3\text{-}23)$$

where $\lambda > 0$, $e = [\phi_d - \phi, \theta_d - \theta, \psi_d - \psi]^T$, and ϕ_d, θ_d, ψ_d are the target angles. Thus, s_q is a 3×1 dimensional matrix:

$$\dot{s_q} = \lambda \dot{e} + D^{-1}(U(t) + \tau(t) + f(t, q, \dot{q})) - \ddot{q}_d \quad (3\text{-}24)$$

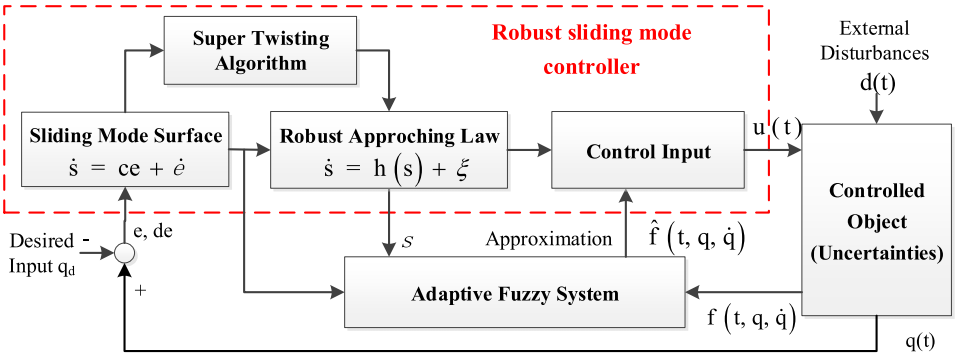

FIGURE 7. Structure of the robust sliding mode algorithm.

It is known that when the sliding mode function $s_q \to 0$, the altitude error e and differential error will converge to zero exponentially. Then we have

$$\begin{aligned} U &= D\ddot{q}_d - D\lambda\dot{e} - f(t,q,\dot{q}) + D\dot{s}_q - \tau(t) \\ D\dot{s}_q &= D\lambda\dot{e} + U + \tau(t) + f(t,q,\dot{q}) - D\ddot{q}_d \end{aligned} \tag{3-25}$$

Here, an improved STA, which inherits the best properties of traditional linear and nonlinear STA in disturbance suppression [38], is introduced as the robust term of SMC to overcome chatters faced by SOSM and increase the robustness of the system to external disturbances:

$$\begin{aligned} \dot{s}_q = -k_1 |s_q|^{\frac{1}{2}} sign(s_q) - k_2 s_q - k_3 \int_0^t sign(s_q)dt \\ -k_4 \int_0^t s_q dt + E_f + \tau_m(t) \end{aligned} \tag{3-26}$$

where $E_f = D^{-1}E$, $\tau_m(t) = D^{-1}\tau(t)$, k_1, k_2, k_3, k_4 are a 3×3 dimensional diagonal matrix, and meet $k_1, k_2, k_3, k_4 > 0$. $D = \begin{bmatrix} I_x & 0 & 0 \\ 0 & I_y & 0 \\ 0 & 0 & I_z \end{bmatrix}$. I_x, I_y, I_z represent the moment of inertia.

Replace $\dot{s}_q$ into Eq. (3-25), and the actual control input is obtained.

$$\begin{aligned} \hat{U} = D\ddot{q}_d - D\lambda\dot{e} - W_q^{*\mathrm{T}}\zeta(q,t) - D(k_1 |s_q|^{\frac{1}{2}} sign(s_q) \\ +k_2 s_q + k_3 \int_{t0}^t sign(s_q)dt + k_4 \int_{t0}^t s_q dt) \end{aligned}$$

Define the Lyapunov function

$$V(t) = \frac{1}{2} s_q^T D s_q + \frac{1}{2\Gamma_q}^T D_q^{-1} \tilde{W}_q \tag{3-27}$$

The differential expression of Eq. (3-27) can be expressed as follows:

$$\begin{aligned} &\dot{V}(t) \\ &= s_q^T D\dot{s}_q + \frac{1}{\Gamma}\tilde{W}_q^T D^{-1}\dot{\hat{W}}_q \\ &= s_q^T \left(D\lambda\dot{e} + \hat{U} - D\ddot{q}_d + f(t,q,\dot{q}) + \tau(t)\right) \\ &\quad + \frac{1}{\Gamma}\tilde{W}_q^T D^{-1}\dot{\hat{W}}_q \\ &= s_q^T(-\tilde{W}_q^T\zeta(q,t) + 2E + \tau(t) - D(k_1 |s_q|^{\frac{1}{2}} sign(s_q) \\ &\quad + k_2 s_q + k_3 \int_{t0}^t sign(s_q)dt \\ &\quad + k_4 \int_{t0}^t s_q dt) + \frac{1}{\Gamma}\tilde{W}_q^T D^{-1}\dot{\hat{W}}_q \\ &= s_q^T D\left(-k_1 |s_q|^{\frac{1}{2}} sign(s_q) - k_2 s_q - k_3 \int_{t0}^t sign(s_q)dt \right. \\ &\quad \left. - k_4 \int_{t0}^t s_q dt + 2E_f + \tau_m(t)\right) \\ &\quad + \tilde{W}_q^T D^{-1}\left(\frac{1}{\Gamma}\dot{\hat{W}}_q - s_q\zeta(q,t)\right) \\ &= \underbrace{-D\left(k_1 |s_q|^{\frac{3}{2}} - k_2 s_q^T s_q - k_3 \int_{t0}^t |s_q| dt - k_4 \int_{t0}^t s_q^T s_q dt\right)}_{Part1} \\ &\quad + \underbrace{s_q^T D\left(2E_f + \tau_m(t)\right)}_{Part2} + \underbrace{\tilde{W}_t^q D^{-1}\left(\frac{1}{\Gamma}\dot{\hat{W}}_q - s_q\zeta(q,t)\right)}_{Part3} \end{aligned} \tag{3-28}$$

Obviously, the first part of $\dot{V}$ meets: $\dot{V}_{Part1} \le 0$ (only when the sliding surface $s_q = 0$, the derivative is zero). Besides, when $\dot{\hat{W}}$ satisfies $\dot{\hat{W}}_q = \Gamma s_q\zeta(q,t)$, $\dot{V}_{Part3} = 0$. Then the original problem is transformed into the derivation of the boundary condition that the sliding surface s_q converges to 0 in $\dot{V}_{Part2}$. Therefore, in order to obtain the uniform convergence time and boundary conditions of k_1, k_2, k_3, k_4, here we introduce three variables ν_1, ν_2 and ν_3

$$\nu = [\nu_1 \nu_2 \nu_3]^T = [|\eta_1|^{\frac{1}{2}} sign(\eta_1)\ \eta_1 \eta_2]^T \tag{3-29}$$

where

$$\begin{aligned} \eta = [\eta_1 \eta_2]^T = [s_q - k_3 \int_0^t sign(s_q)dt \\ -k_4 \int_0^t s_q dt + \tau_m(t)]^T \end{aligned}$$

Then

$$\begin{cases} \dot{\nu}_1 = \dfrac{1}{2|\nu_1|}(-k_1\nu_1 - k_2\nu_2 + \nu_3 + E_f) \\ \dot{\nu}_2 = -k_1\nu_1 - k_2\nu_2 + \nu_3 + E_f \\ \dot{\nu}_3 = \dfrac{1}{|\nu_1|}(-k_3\nu_1) - k_4\nu_2 + \dot{\tau}_m(t) \end{cases} \tag{3-30}$$

Define the Lyapunov function

$$V_1(\nu) = 2k_3\nu_1^2 + \frac{1}{2}\nu_2^2 + \frac{1}{2}\nu_3^2 + \frac{1}{2}(k_1\nu_1 + k_2\nu_2 - \nu_3)^2 \tag{3-31}$$

When introducing

$$P = \frac{1}{2}\begin{bmatrix} 4k_3+k_1^2 & k_1k_2 & -k_1 \\ k_1k_2 & 2k_4+k_2^2 & -k_2 \\ -k_1 & -k_2 & 2 \end{bmatrix}, \quad A^TP+PA = -Q,$$

then $V_1(\nu)$ can be transformed into the positive definite quadratic form:

$$V_1(\nu) = \nu^T P\nu$$

The corresponding derivative of the Lyapunov equation is obtained as follows:

$$\begin{aligned}\dot{V}_1(\nu) &= -\nu^T\left(A^TP + PA\right)\nu + 2\nu^T PB \\ &= -\nu^T Q_1\nu - \frac{1}{|s_q|^{\frac{1}{2}}}\nu^T Q_2\nu - M_1\nu - \frac{1}{|s_q|^{\frac{1}{2}}}M_2\nu\end{aligned} \tag{3-32}$$

where $Q = Q_1 + Q_2$, $B = [E_f, E_f, \dot{\tau}_m]^T$,

$$M_1 = \frac{1}{2}[-\left(k_1^2+4k_3\right)E_f + k_1\dot{\tau}_m - k_1k_2E_f + k_2\dot{\tau}_m k_1E_f - 2\dot{\tau}_m]$$

$$M_2 = \frac{1}{2}E_f[-k_1k_2 - \left(k_2^2+2k_4\right)k_2]$$

$$Q_1 = \frac{1}{2}\begin{bmatrix} -k_1^2k_2 & -k_1\left(k_2^2+k_4\right) & k_1k_2 \\ -k_1\left(k_2^2+k_4\right) & -k_2\left(k_2^2+2k_4\right) & k_2^2+k_4 \\ k_1k_2 & k_2^2+k_4 & -k_2 \end{bmatrix},$$

$$Q_2 = \frac{1}{2}\begin{bmatrix} -k_1^3-2k_1k_3 & k_1k_4 - k_2\left(k_1^2+k_3\right) & k_1^2 \\ k_1k_4 - k_2\left(k_1^2+k_3\right) & 2k_2k_4 - k_1k_2^2 & k_1k_2 - 2k_4 \\ k_1^2 & k_1k_2 - 2k_4 & -k_1 \end{bmatrix}$$

For some constants $\tau_1, \tau_2, E_1, E_2 \geq 0$, if E_f and $\dot{\tau}$ meet $|E_f| < E_1|s_q|^{\frac{1}{2}} + E_2|s_q|$, $|\dot{\tau}_m| < \tau_1 + \tau_2|s_q|$, the below restriction can be obtained

$$\frac{1}{|s_q|^{\frac{1}{2}}}M_2\nu \leq \frac{E_1}{|s_q|^{\frac{1}{2}}}\nu^T\triangle_1\nu + E_2\nu^T\triangle_1\nu \tag{3-33}$$

$$M_1\nu \leq \frac{1}{|s_q|^{\frac{1}{2}}}\nu^T\triangle_2\nu + \nu^T\triangle_3\nu \tag{3-34}$$

where

$$\triangle_1 = \frac{1}{2}\begin{bmatrix} -k_1k_2 & 0 & -\frac{k_2}{2} \\ 0 & -\left(k_2^2+2k_4\right) & 0 \\ -\frac{k_2}{2} & 0 & 0 \end{bmatrix}$$

$$\triangle_2 = \frac{1}{2}\begin{bmatrix} k_1\tau_1 & 0 & 0 \\ 0 & -\left(k_1^2+4k_3\right)E_2 - k_1\tau_2 - k_1k_2E_1 & 0 \\ 0 & 0 & 0 \end{bmatrix}$$

$$\triangle_3 = -\frac{1}{2} \times \begin{bmatrix} \left(k_1^2+4k_3\right)E_1 - k_1\tau_1 & 0 & \frac{k_1E_1+2\tau_1}{2} \\ 0 & k_1k_2E_2 - k_2\tau_2 & \frac{k_1E_2+2\tau_2}{2} \\ \frac{k_1E_1+2\tau_1}{2} & \frac{k_1E_2+2\tau_2}{2} & 0 \end{bmatrix}$$

In this case, $\dot{V}_1(\nu)$ can be further expressed as

$$\dot{V}_1(\nu) \leq -\nu^T\Gamma_1\nu - \frac{1}{|s_q|^{\frac{1}{2}}}\nu^T\Gamma_2\nu \tag{3-35}$$

where $\Gamma_1 = Q_1 + \triangle_3 + E_2\triangle_1$, $\Gamma_2 = Q_2 + \triangle_2 + E_2\triangle_1$.

According to system stability conditions, when Γ_1 and Γ_2 are positive definite matrices, the system converges uniformly.

$$Q_1 + \triangle_3 + E_2\triangle_1 > 0 \tag{3-36}$$

$$Q_2 + \triangle_2 + E_2\triangle_1 > 0 \tag{3-37}$$

Therefore, based on equations (3-36) and (3-37), the boundary conditions of k_1, k_2, k_3, k_4 satisfying Eq. (3-38) [38]:

where $p_1 = k_1\left(\frac{1}{4}k_1^2 - \tau_1\right) + \frac{1}{2}(k_1 - E_1)(2k_3 + \frac{1}{2}k_1^2)$.

As predefined in Eq. (3-33), in the boundary conditions, parameters τ_1 and τ_2 are two constants and used to restrict the external disturbances $\tau(t)$. With the bounded external disturbance in actual flight environment, and it is easy to estimate this boundary τ_1, τ_2 using expert experience or measurement. In this way, k_1, k_2, k_3 and k_4 can be obtained.

Subsequently, we have

$$\begin{aligned}\dot{V}_1(\nu) &\leq -\frac{1}{|s_q|^{\frac{1}{2}}}\lambda_{min}\{\Gamma_1\}\|\nu\|^2 - \lambda_{min}\{\Gamma_2\}\|\nu\|^2 \\ &\leq -\alpha_1V_1^{\frac{1}{2}}(\nu) - \alpha_2V_1(\nu)\end{aligned} \tag{3-39}$$

where

$$\alpha_1 = \left(\lambda_{min}^{1/2}\{P\}\lambda_{min}\{\Gamma_1\}\right)/\lambda_{max}\{P\} \tag{3-40}$$

$$\alpha_2 = \left(\lambda_{min}\{\Gamma_2\}\right)/\lambda_{max}\{P\} \tag{3-41}$$

$\lambda_{min}\{\cdot\}$ and $\lambda_{max}\{\cdot\}$ represent the minimum and maximum eigenvalues of the symmetric matrix.

Finally, the Lyapunov function satisfies $\dot{V}_1 \leq 0$ (only when the sliding surface $\nu = 0$, the derivative $\dot{V}_1$ equals to zero), that is, the sliding surface s_q, attitude error e and differential error $\dot{e}$ will converge uniformly to zero in finite-time at exponential speed. Then part 2 of derivative $\dot{V}$ in Eq. (3-28) meets $\dot{V}_{Part2} = s_q^TD\left(E_f + \tau_m(t)\right) \to 0$, namely:

$$\begin{aligned}\dot{V}(t) =& \underbrace{-D\left(k_1|s_q|^{\frac{3}{2}} - k_2s_q^Ts_q - k_3\int_{t0}^{t}|s_q|\,dt - k_4\int_{t0}^{t}s_q^Ts_q dt\right)}_{Part1} \\ &+ \underbrace{s_q^TD\left(E_f + \tau_m(t)\right)}_{Part2} + \underbrace{\tilde{W}_t^qD^{-1}\left(\frac{1}{\Gamma}\dot{\hat{W}}_q - s_q\zeta(q,t)\right)}_{Part3} < 0,\end{aligned}$$

with the boundary conditions of k_1, k_2, k_3, k_4 in Eq. (3-38), as shown at the bottom of the next page.

Furthermore, the computing complexity of intelligent and robust parts in this proposed controller can be derived as follows:

$$\begin{aligned} T(m,n,w) &= \overbrace{O(m^*n^*3}^{\text{Fuzzy Logic}} + \overbrace{m^*n+3}^{\text{Adaptiveness}} + \overbrace{3^*W \wedge 2+w)}^{\text{STA}} \\ &= O(m^*n+w \wedge 2) \end{aligned}$$

According to this formula, the growth of computing complexity is related to m, n and w, which represent the elements number of fuzzy set A1, A2 (Section 3.2) and controlling variables (such as θ, φ, ψ), respectively. The complexity mainly comes from multiplication and addition, and there is no complex power operation and exponential operation.

C. STABILITY ANALYSIS OF CLOSED-LOOP SYSTEM

Here, the model uncertainties in x, y, z dimensions are [23] $\chi_1(t,x,\dot{x})$, $\chi_2(t,y,\dot{y})$, $\chi_3(t,z,\dot{z})$, and $\xi(t,q,\dot{q})$ denotes nonlinear uncertainties of inner attitude subsystem, i.e., the vibration and the ignorance structure of the airframe; $\gamma(t)$ denotes the external disturbances of the control system, where $\gamma_1(t)$, $\gamma_2(t)$, $\gamma_3(t)$ are components of $\gamma(t)$ in x, y, z directions. $\tau(t) = [\tau_\varphi(t), \tau_\theta(t), \tau_\psi(t)]^T \in \mathbb{R}^{3\times1}$ denotes the disturbance to the built-in gyroscope. $\delta_1(t,x,\dot{x}) = \chi_1(t,x,\dot{x}) + \gamma_1(t)$, $\delta_2(t,y,\dot{y}) = \chi_2(t,y,\dot{y}) + \gamma_2(t)$, $\delta_3(t,z,\dot{z}) = \chi_3(t,z,\dot{z}) + \gamma_3(t)$.

Based on the above controller design, define the Lyapunov function of quadrotor system as

$$V = \frac{1}{2}s_x^2 + \frac{1}{2}s_y^2 + \frac{1}{2}s_z^2 + \frac{1}{2}s_q^T D s_q + \frac{1}{2\Gamma}\tilde{W}_q^T D^{-1}\tilde{W}_q$$

Then

$$\begin{aligned} \dot{V} &= s_x\dot{s}_x + s_y\dot{s}_y + s_z\dot{s}_z + s_q^T D\dot{s_q} + \frac{1}{\Gamma}\tilde{W}_q^T D^{-1}\dot{\hat{W}}_q \\ &= s_x\left(c_x\dot{e}_{1x} + \dot{e}_{2x}\right) + s_y\left(c_y\dot{e}_{1y} + \dot{e}_{2y}\right) + s_z\left(c_z\dot{e}_{1z} + \dot{e}_{2z}\right) \\ &\quad + s_q^T D\dot{s_q} + \frac{1}{\Gamma}\tilde{W}_q^T D^{-1}\dot{\hat{W}}_q \\ &= s_x\left[c_x\left(x_2 - \dot{x}_{1d}\right) + \frac{1}{m}U_x - \frac{K_{ax}}{m}x_2 - \ddot{x}_{1d} + J_1\dot{e}_1 + J_0e_1\right] \\ &\quad + s_y\left[c_y\left(y_2 - \dot{y}_{1d}\right) + \frac{1}{m}U_y - \frac{K_{ay}}{m}y_2 - \ddot{y}_{1d} + J_3\dot{e}_1 + J_2e_1\right] \\ &\quad + s_z\left[c_z\left(z_2 - \dot{z}_{1d}\right) + \frac{1}{m}U_z - \frac{K_{az}}{m}z_2 - \ddot{z}_{1d} + J_5\dot{e}_1 + J_4e_1\right] \\ &\quad + s_q^T\left(\hat{U} - D\lambda\dot{e} - D\ddot{q}_d + f(t,q,\dot{q})\right) + \frac{1}{\Gamma}\tilde{W}_q^T D^{-1}\dot{\hat{W}}_q \end{aligned}$$

where $c_x, c_y, c_z > 0$ denote the convergence parameters of the sliding surface s_x, s_y, s_z; constants $J_0, J_1, J_2, J_3, J_4, J_5 > 0$. According to the virtual variables in U_x, U_y, U_z Eq. (3-11), (3-13) and (3-14), for parameters $\rho_1 > \frac{\delta_1^u}{m}$, $\rho_3 > \frac{\delta_2^u}{m}$, $\rho_1 > \frac{\delta_3^u}{m}$, where δ_1^u, δ_2^u and δ_3^u is the upper bound of disturbance $\delta_1(t,x,\dot{x})$, $\delta_2(t,y,\dot{y})$, $\delta_3(t,z,\dot{z})$; $\rho_2, \rho_4, \rho_6 > 0$, $\dot{\hat{W}}_q = \Gamma s_q\zeta(q,t)$.

The control laws satisfy the following equations:

$$\begin{aligned} U_1 &= (K_{ay}z_2 + m(\ddot{z}_{1d} + c_y(J_5e_{1y} + J_4\int_0^t e_{1z}(\tau)\,d\tau - e_{2z}) \\ &\quad -(J_5\dot{e}_{1z} + J_4e_{1z}) - \rho_5 sign(s_z) + \rho_6 s_z) \\ &\quad + mg)/(cos\varphi_d cos\theta_d) \\ U_2 &= I_x\ddot{\varphi}_d - I_x\lambda_\varphi\dot{e}_\varphi - \hat{f}(t,\varphi_d,\dot{\varphi}_d) - I_x(k_{1\varphi}|s_\varphi|^{\frac{1}{2}}sign(s_\varphi) \\ &\quad + k_{2\varphi}s_\varphi + k_{3\varphi}\int_{t0}^t sign(s_\varphi)dt + k_{4\varphi}\int_{t0}^t s_\varphi dt) \\ U_3 &= I_y\ddot{\theta}_d - I_y\lambda_\theta\dot{e}_\theta - \hat{f}(t,\theta_d,\dot{\theta}_d) - I_y(k_{1\theta}|s_\theta|^{\frac{1}{2}}sign(s_\theta) \\ &\quad + k_{2\theta}s_\theta + k_{3\theta}\int_{t0}^t sign(s_\theta)dt + k_{4\theta}\int_{t0}^t s_\theta dt) \\ U_4 &= I_z\ddot{\psi}_d - I_z\lambda_\psi\dot{e}_\psi - \hat{f}(t,\psi_d,\dot{\psi}_d) \\ &\quad - I_y(k_{1\psi}|s_\psi|^{\frac{1}{2}}sign(s_\psi) + k_{2\psi}s_\psi \\ &\quad + k_{3\psi}\int_{t0}^t sign(s_\psi)dt + k_{4\psi}\int_{t0}^t s_\psi dt) \end{aligned}$$

where $\lambda_\varphi, \lambda_\theta, \lambda_\psi > 0$ denote the convergence parameters of the sliding surface s_φ, s_θ, s_ψ; $\theta_d = arctan\left((U_xcos\psi + U_ysin\psi)/U_z\right)$, $\psi_d = arctan\left(cos\theta(U_xsin\psi - U_ycos\psi)/U_z\right)$; $k_{i\varphi} = k_{i\theta} = k_{i\psi}$ and $k_i = \begin{bmatrix} k_{i\varphi} & 0 & 0 \\ 0 & k_{i\theta} & 0 \\ 0 & 0 & k_{i\psi} \end{bmatrix}$ (i = 1,2,3,4) meet the condition of Eq. (3-38). The derivative of Lyapunov function can be rewritten as

$$\begin{aligned} \dot{V} = -\rho_1|s_x| - \rho_2 s_x^2 - \rho_3|s_y| - \rho_4 s_y^2 - \rho_5|s_z| - \rho_6 s_z^2 \\ + W_q^T D^{-1}\left(\frac{1}{\Gamma}\dot{\hat{W}}_q - s_q\zeta(q,t)\right) \end{aligned}$$

Obviously, when $\dot{\hat{W}}$ satisfies $\dot{\hat{W}}_q = \Gamma s_q\zeta(q,t)$, the derivative of V is no more than 0, and only when the sliding surface s_x, s_y, s_z equal to zero, the derivative is zero. Therefore,

$$\begin{cases} k_1 > 2\max(E_1, \sqrt{\tau_1}) \\ k_2 > \frac{3}{8}E_2 + \frac{1}{4}\sqrt{\frac{9}{4}E_2^2 + 8\tau_2} \\ k_3 > \frac{E_1k_1^2 + \frac{1}{8}E_2^2k_1 + \tau_1k_1}{k_1 - 2E_1} \\ k_4 > \frac{k_1\left[\frac{1}{2}k_1\left(k_1 + \frac{1}{2}E_2\right)^2(2k_2^2 + \frac{3}{2}E_2k_2 + \tau_2) + (\frac{5}{2}k_2^2 + \frac{3}{2}E_2k_2 + \tau_2)p_1\right]}{k_1(p_1 - \frac{1}{2}k_1^3)} \end{cases} \quad (3\text{-}38)$$

according to Lyapunov stability theory, the overall closed-loop system of quadrotor UAV is stable. In the above stability analysis, the range of each parameter is explained in detail, so the parameters related to the controller can be obtained by taking values in its definition domain. With the detailed definition domain of each parameter, the appropriate parameter values can be obtained by the intelligent heuristic algorithms combining with the idea of experience adjustment and iteration, which determine the appropriate parameter value effectively by defining the objective function. Here we mainly used particle swarm optimization (PSO) [42], [43]. Several rules are given in tuning controller parameters:

1) By taking the minimum regulation time and overshoot as the objective function, PSO is used to search the parameters in the definition domain i.e., super twisting parameters k_1, k_2, k_3, k_4, nonnegative real parameters J_0, J_1, ρ_1, ρ_2, etc., until the values satisfying iteration times and minimum threshold of objective function;

2) As PSO is used to optimize the parameters, the selection of learning rate and inertia weight has a great influence on the particle velocity in the parameter search space. An effective method is to start with a large learning rate and gradually reduce the speed until the objective function is no longer divergent.

3) While gradually improving the learning rate of each small batch (iteration), a feasible way is conducted to observe and record the change of the objective function after each increment.

4) In order to improve the efficiency of parameter optimization, for several parameters, i.e., J_0, J_1, ρ_1, ρ_2, as long as their values are greater than 0, the stability conditions will meet. An effective way to tuning those parameters are increasing the value of these parameters empirically, as the simulation of W_q demonstrated in section IV.

IV. SIMULATION AND RESULTS

In this section, several case studies were conducted by introducing three commonly used control algorithms. This was done to verify the effectiveness of the elaborated control strategy. The parameters of the quadrotor aircraft used in the simulations (Table 2) are also referenced in the literature [11].

A. EXAMPLE 1 ATTITUDE TRACKING SIMULATION

To illustrate the robustness and convergence performance of the proposed fuzzy adaptive sliding mode controller, we take the attitude subsystem and conduct a contrast simulation on its attitude tracking effect and input stability.

(1) Cascade PID controller (PID) [14]

(2) Improved sliding mode controller (M-SOSM) [23]

(3) Fuzzy sliding mode controller (Fuzzy M-SOSM)

(4) Elaborated fuzzy adaptive sliding mode controller (AdapFuzzy M-SOSM)

Among these three controllers, the cascade PID controller contains a double-loop PID control strategy for both angle and angular velocity. The SMC applied in M-SOSM controller and Fuzzy M-SOSM is optimized by the improved super twisting algorithm (STA), which is the same as the robust term applied in the proposed fuzzy adaptive M-SOSM controller. This was also done to demonstrate the anti-interference robustness and online approximation performance. The model uncertainties of attitude subsystem are chosen as:

$$\xi(t, q, \dot{q}) = 0.3\dot{q}(t) + 0.2q(t) + 0.3$$

As illustrated in Eqs. (4-1) and (4-2), the multi-frequency function $u(t)$ and sine signal $\tau(t)$ are introduced as the changing frequency reference signal and the high-frequency dynamic external disturbances, respectively.

$$r(t) = \sin t + \sin(2t) + sin(3t) \quad (4\text{-}1)$$

$$\tau(t) = 0.2sin40\pi t \quad (4\text{-}2)$$

Based on the control design procedure in Section 3, and the simulation examples in the literature [14], the parameters used in this contrast simulation are listed in Table 3.

TABLE 2. Parameters of the quadrotor aircraft.

Variable	Value	Units
m	0.23	kg
g	9.8	m/s^2
l	0.23	m
Ix=Iy	7.5e-3	Ns^2/rad
Iz	1.3e-2	Ns^2/rad
Ir	6e-5	Ns^2/rad
$K_{ax}=K_{ay}=K_{az}$	0.012	Ns/m
b	7.5e-7	Ns^2
d	3.13e-5	N/ms^2

TABLE 3. Controller parameters used in the simulations.

Para.	Value	Para.	Value
γ	1500	E	[0.64 0.64 0.64]
k1	$1 * eye(3)$	η	15
k2	$1 * eye(3)$	ε	$[0.64; 0.64; 0.64]^T$
k3	$1 * eye(3)$	c1	[-1 -0.5 0 0.5 1]
k4	$6 * eye(3)$	c2	[-1 -0.5 0 0.5 1]
λ	$3 * eye(3)$	x_i	$[-\pi/3, \pi/3]$
k_{p1}	$[10\ 10\ 10]^T$	k_{p2}	$[10\ 10\ 10]^T$
k_{i1}	$[0.03\ 0.03\ 0.03]^T$	k_{i2}	$[0.03\ 0.03\ 0.03]^T$
k_{d1}	$[0.01\ 0.01\ 0.01]^T$	k_{d2}	$[0.01\ 0.01\ 0.01]^T$

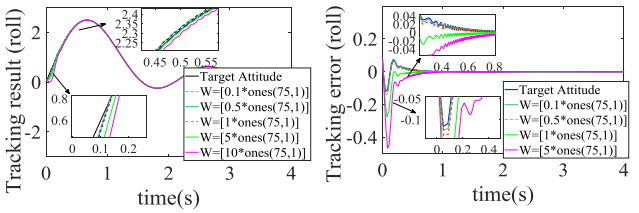

FIGURE 8. Attitude tracking and tracking errors with different initial value of W_q (roll angle φ).

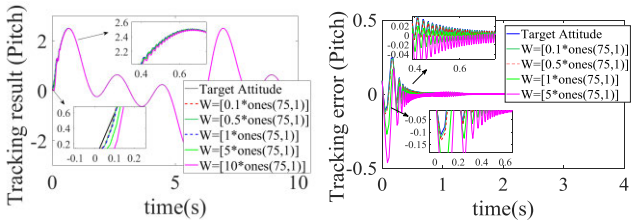

FIGURE 9. Attitude tracking and tracking errors with different initial value of W_q (pitch angle θ).

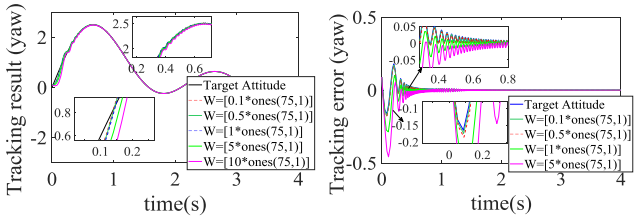

FIGURE 10. Attitude tracking and tracking errors with different initial value of W_q (yaw angle ψ).

The fuzzy membership functions are illustrated as follows

$$\mu = \begin{cases} \mu_{NM}(x_i) = exp\left\{-\left[(x_i + \pi/3) / (\pi/12)\right]^2\right\} \\ \mu_{NS}(x_i) = exp\left\{-\left[(x_i + \pi/6) / (\pi/12)\right]^2\right\} \\ \mu_{Z}(x_i) = exp\left\{-\left[x_i / (\pi/12)\right]^2\right\} \\ \mu_{PS}(x_i) = exp\left\{-\left[(x_i - \pi/6) / (\pi/12)\right]^2\right\} \\ \mu_{PM}(x_i) = exp\left\{-\left[(x_i - \pi/3) / (\pi/12)\right]^2\right\} \end{cases}$$

where $x_i \in \left[-\frac{\pi}{3}, \frac{\pi}{3}\right]$.

To obtain the appropriate initial parameters of the designed controller, we first analyzed the influence of parameter W_q on tracking performance under different initial values through some of the simulations.

According to Figs. 8-10, before the tracking process is stable, the tracking effect decreases with increases of the initial value. However, it has no effect on the tracking convergence time. This means that in the selection of the initial value, we should try to choose a smaller initial value for W_q. Thus, we chose $W_q = [0.1 * ones(3 * 25, 1)]$ to conduct the following two simulations.

The attitude tracking result and tracking errors of those three control strategies are shown in Fig. 11-13. From those figures, the introduction of improved super twisting

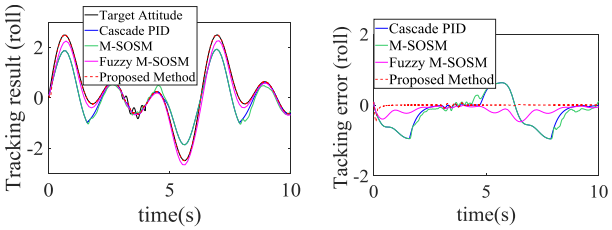

FIGURE 11. Attitude trajectory tracking and tracking errors (roll angle φ).

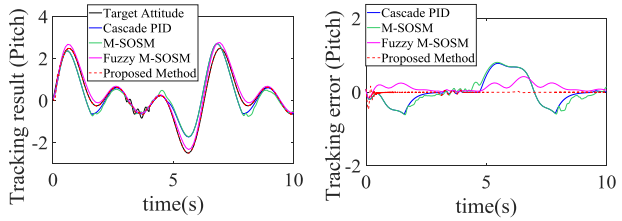

FIGURE 12. Attitude trajectory tracking and tracking errors (pitch angle θ).

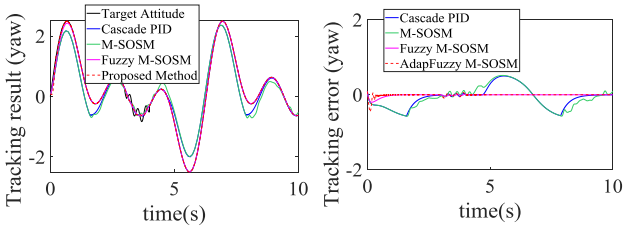

FIGURE 13. Attitude trajectory tracking and tracking errors (yaw angle ψ).

algorithm can alleviate the high-frequency disturbances effectively. In addition, when compared with M-SOSM and Fuzzy M-SOSM, the tracking error of the proposed controller was reduced very quickly, converging to zero in 0.5 s. This means that the tracking accuracy was highly improved with the introduction of adaptive law and fuzzy system. According to the illustrated information and when compared with the PID cascade controller and second order sliding mode controller, the elaborated adaptive control strategies demonstrated a quite satisfactory tracking effect after only an extremely tiny adjustment in time (nearly 0.6 s). Moreover, the tracking errors for the other algorithms were bounded in and $[-0.7, 0.4]$, $[-0.3, 0.3]$ and $[0, 0.3]$, respectively.

The root mean square errors (RMSE) of this contrast simulation are quantitatively summarized in Table 4. Given these results and when compared with the cascade PID, M-SOSM and fuzzy M-SOSM, the designed controller had significantly faster convergence and stability performance in its attitude tracking stability.

B. EXAMPLE 2 TRAJECTORY TRACKING SIMULATION

Here, the trajectory tracking simulation was conducted to demonstrate the validity and mobility of the elaborated control strategy. The object trajectory used was a cylindrical spiral, as shown in Eq. (4-3) [34].

$$\begin{cases} x_d = 1.5cos(0.5t) \\ y_d = 1.5cos(0.5t) \\ z_d = t \\ \psi_d = 60^\circ \end{cases} \tag{4-3}$$

TABLE 4. Quantitative comparison of tracking performance.

Method	RMSE (φ)	RMSE (θ)	RMSE (ψ)
Cascade PID	0.3325	0.2747	0.2456
M-SOSM	0.2359	0.2359	0.1661
Fuzzy M-SOSM	0.1359	0.1175	0.0535
AdapFuzzy M-SOSM	**0.0068**	**0.0072**	**0.0067**

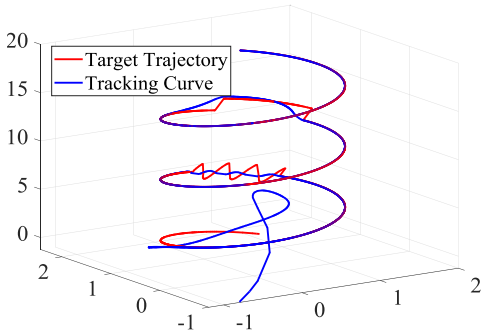

FIGURE 14. Trajectory tracking result.

The simulation time is 20s, initial position coordinates and attitude of the quadrotor were set as $[x, y, z] = [000]$, $[\phi, \theta, \psi] = [000]$. Denoting the model uncertainty $\chi(t)$ as

$$\chi(t) = [0.1\dot{x}(t) + 0.2, 0.1\dot{y}(t) + 0.2, 0.1\dot{z}(t) + 0.2]^T$$

In general, it is difficult to control the aircraft under high-frequency random disturbances and multi-frequency random disturbances. Here, to solve this problem, two forms of wind gusts were presented in the simulation: high frequency random disturbances (high frequency sine signal) [17], [27], [35], [36] and multi frequency random disturbances (square wave signal) [34], [37]. The disturbances used in this tracking simulation consist of the following two parts:

$$\gamma(t) = \begin{cases} 0.2sin\,40\pi t, & t \in [7, 8] \\ 1, & t \in [13, 14] \end{cases}$$
$$\tau(t) = 0.1sin\,t$$

According to the literature [3], the parameter cx does not affect the stability of the control system but has a direct relationship with the convergence time. If the parameter cx is too large, the fast convergence speed will produce strong buffeting; if the parameter a is too small, the convergence time will be longer. Therefore, in this simulation, we used the empirical value of $cx = 5$. The fuzzy basis vector for both altitude and attitude controllers were $w = [0.1 * ones(75, 1)]$ and $w = [zeros(25, 1)]$. Moreover, the domain of each parameter and the fuzzy membership function used were the same as in Section 4.1.

Fig. 14 illustrates the trajectory tracking results. The elaborated control algorithms displayed a satisfactory tracking

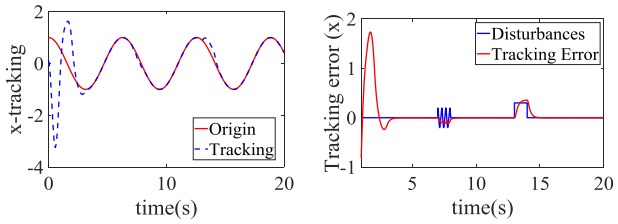

FIGURE 15. Trajectory tracking and errors in x-direction.

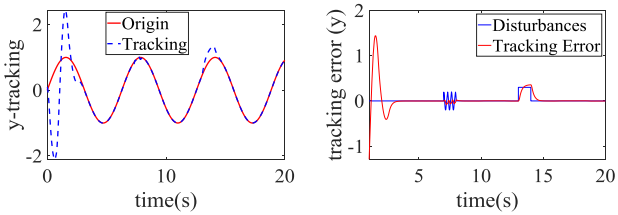

FIGURE 16. Trajectory tracking and errors in y-direction.

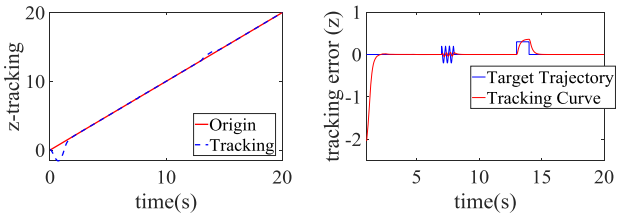

FIGURE 17. Trajectory tracking and errors in z-direction.

accuracy and robust performance against the model uncertainties and disturbances. Despite the initial difference in the beginning of the simulation between these two lines, the control system converged quickly to track the cylindrical spiral trajectory. The trajectory tracking errors are displayed in Figs. 15-17.

According to the results presented above, when the high-frequency appeared in [7s,8s], the position response of the quadrotor UAV experienced a fluctuated trend with a remarkably small amplitude ($\leq$0.1m). Then in time interval [13s,14s], although the step disturbances influenced the tracking accuracy in short time range, the tracking errors reduced quickly ($\leq$0.2 s) after the external interference disappeared.

Here, in order to increase the credibility of simulation results, the confidence level of tracking errors in x-, y-, z-directions are evaluated. The main indicators involve the mean value (Mean), standard deviation (SD), and the corresponding confidence interval (CI) of them at 0.95 confidence level. Table 5 shows confidence levels in x, y, z directions under model uncertainties and external disturbances.

In this simulation, the upper and lower limits of the external disturbance are [−0.2m,1m], and the width of the interference interval is 1.2m. From table 5, the confidence interval width of the control system in x, y, z directions are 0.0144m, 0.0094m and 0.0070m, accounting for 1.2%, 0.78% and 0.58% of the interference interval width, respectively. It demonstrates that the simulation results have high accuracy and reliability at 95% confidence level.

TABLE 5. Confidence levels (95%) in x, y, z directions.

Dim.	Mean	SD	CI of Mean	CI of SD
x	0.0299	0.2583	[0.0227, 0.0371]	[0.2533, 0.2635]
y	0.0196	0.1681	[0.0149, 0.0243]	[0.1648, 0.1715]
z	0.0164	0.1263	[0.0129, 0.0199]	[0.1239, 0.1289]

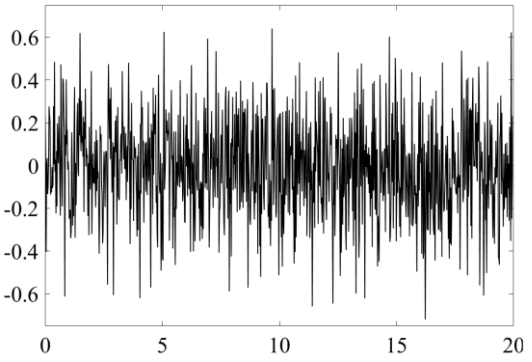

FIGURE 18. Gaussian white noise used in the simulation.

C. EXAMPLE 3 TRACKING SIMULATION WITH MEASUREMENT NOISE

Since the practical factors such as measurement noise and navigation error can affect the control performance to some extent, additional tracking simulation is conducted to demonstrate the effectiveness of the elaborated control strategy with random noise. In this simulation, the related parameters such as simulation time, initial position coordinates, target trajectory, model uncertainties, external disturbances etc., are the same as Section 4.2.

As shown in Fig. 18, the random noise υ is introduced to simulate measurement noise and navigation error in real environment. Referring to the treatment of measurement error in some literatures [44], [45], when ignoring factors such as measurement technology, human and instruments, the value and symbol of measurement error change randomly in an unpredictable way, and obey normal distribution. Therefore, in the simulation, we selected Gaussian white noise as the measurement noise, which is subjected to normal distribution of 0-mean value and 0.05-variance. The noise generated by random number generator with the sampling period of 0.001s. Fig. 19 illustrates the trajectory tracking results.

Compared with Fig. 14, it is clear that despite the existing of gaussian random noise, the control system presents a stable tracking performance and converges quickly to track the cylindrical spiral trajectory. The trajectory tracking errors are displayed in Figs. 20-22.

According to the results above, the position response of the quadrotor to the random noise and external disturbances experienced a fluctuated trend with a remarkably small amplitude (bounded in $\pm$0.1m), which demonstrates

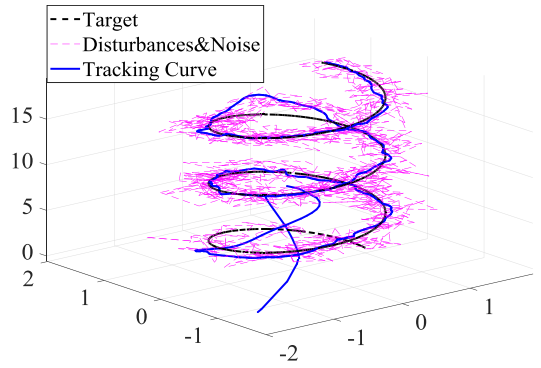

FIGURE 19. Trajectory tracking result with random noise.

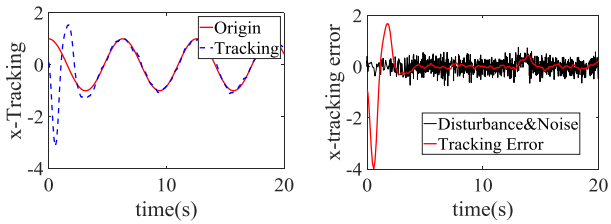

FIGURE 20. Trajectory tracking and errors in x-direction.

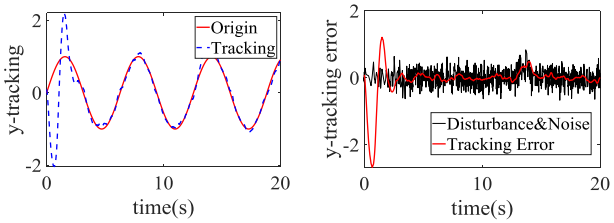

FIGURE 21. Trajectory tracking and errors in y-direction.

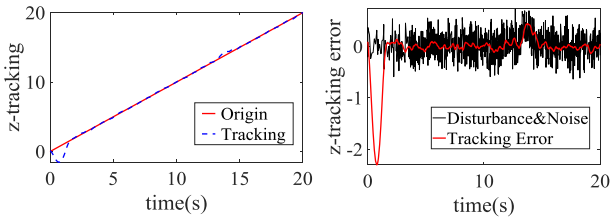

FIGURE 22. Trajectory tracking and errors in z-direction.

the effectiveness of the proposed controller on alleviation of the random noise. Table 6 illustrates the confidence indicators in x, y, z directions with random noise at 0.95 confidence level.

As shown in table 6, compared with Example 2, the confidence interval width of the control system in x, y, z directions are expanded to some extent (0.0541m, 0.0328m and 0.0292m) due to the gaussian random noise. However, the upper and lower bounds of the total interference also increase from 1.2m to 2.4m, and the ratio of the confidence interval to the total disturbance width of the system is 2.25%, 1.37%, 1.22%, bounded in 2.5%, which denotes that the control strategy designed in this paper can effectively suppress the random noise.

TABLE 6. Confidence levels (95%) in x, y, z directions under random measurement noise.

Dim.	Mean	SD	CI of Mean	CI of SD
x	0.0007	0.3629	[-0.0213, 0.0228]	[0.3480, 0.3792]
y	0.0060	0.2698	[-0.0104, 0.0224]	[0.2587, 0.2819]
z	-0.0064	0.2408	[-0.0210, 0.0082]	[0.2309, 0.2516]

V. CONCLUSION

In this paper, we developed a combinatorial adaptive sliding mode control strategy combined with fuzzy algorithm and sliding mode control algorithm for quadrotor UAVs to guarantee their tracking accuracy and robust performance. The controller considered not only the underactuated and strongly coupled characteristics of the quadrotor, but also the dynamic model uncertainties and external disturbances. The overall system was divided in the outer-loop position subsystem and inner-loop attitude subsystem, upon which the corresponding controllers were proposed according to the specific structure of subsystems. In case studies, the time-varying model uncertainties and multi-frequency external disturbances were introduced to illustrate the response performance for changing frequency nonlinearities. As a result, the first comparative simulation allowed us to conclude that, when compared with the cascade PID, M-SOSM and fuzzy SOSM controllers, the proposed fuzzy adaptive M-SOSM control strategy had the smallest error on both attitude and speed tracking. Furthermore, the validity and mobility of the elaborated control strategy was demonstrated by the second trajectory tracking simulation.

With the increasing demand across a variety of fields for autonomous and intelligent flights using UAVs, our future work will entail more in-depth research into the global optimization of control parameters as well as the development of a robust control algorithm with memory function and a tracking control strategy based on data fusion. This work will be critical, since they form the basis for autonomous flight control of UAVs. We will also validate the algorithm using actual hardware experiments in a real flight environment.

REFERENCES

[1] E. Kayacan and R. Maslim, "Type-2 fuzzy logic trajectory tracking control of quadrotor VTOL aircraft with elliptic membership functions," *IEEE/ASME Trans. Mechatronics*, vol. 22, no. 1, pp. 339–348, Feb. 2017.

[2] X. Wang and B. Shirinzadeh, "Nonlinear augmented observer design and application to quadrotor aircraft," *Nonlinear Dyn.*, vol. 80, no. 3, pp. 1463–1481, May 2015.

[3] J. Zhang, D. Gu, C. Deng, and B. Wen, "Robust and adaptive backstepping control for hexacopter UAVs," *IEEE Access*, vol. 7, pp. 163502–163514, Nov. 2019.

[4] H. Yang, L. Cheng, Y. Xia, and Y. Yuan, "Active disturbance rejection attitude control for a dual closed-loop quadrotor under gust wind," *IEEE Trans. Control Syst. Technol.*, vol. 26, no. 4, pp. 1400–1405, Jul. 2018.

[5] N. Ahmed, M. Chen, and S. Shao, "Disturbance observer based tracking control of quadrotor with high-order disturbances," *IEEE Access*, vol. 8, pp. 8300–8313, 2020.

[6] S. Islam, P. X. Liu, and A. El Saddik, "Robust control of four-rotor unmanned aerial vehicle with disturbance uncertainty," *IEEE Trans. Ind. Electron.*, vol. 62, no. 3, pp. 1563–1571, Mar. 2015.

[7] J. Liu, H. An, Y. Gao, C. Wang, and L. Wu, "Adaptive control of hypersonic flight vehicles with limited angle-of-attack," *IEEE/ASME Trans. Mechatronics*, vol. 23, no. 2, pp. 883–894, Apr. 2018.

[8] B. Qiu, G. Wang, Y. Fan, D. Mu, and X. Sun, "Adaptive course control-based trajectory linearization control for uncertain unmanned surface vehicle under rudder saturation," *IEEE Access*, vol. 7, pp. 108768–108780, Aug. 2019.

[9] M. He and J. He, "Extended state observer-based robust backstepping sliding mode control for a small-size helicopter," *IEEE Access*, vol. 6, pp. 33480–33488, Jun. 2018.

[10] Q. Shen, B. Jiang, and V. Cocquempot, "Adaptive fault-tolerant backstepping control against actuator gain faults and its applications to an aircraft longitudinal motion dynamics," *Int. J. Robust Nonlinear Control*, vol. 23, no. 15, pp. 1753–1779, Oct. 2013.

[11] S. Mobayen, "An adaptive fast terminal sliding mode control combined with global sliding mode scheme for tracking control of uncertain nonlinear third-order systems," *Nonlinear Dyn.*, vol. 82, nos. 1–2, pp. 599–610, Oct. 2015.

[12] J. Zhang, Z. Ren, C. Deng, and B. Wen, "Adaptive fuzzy global sliding mode control for trajectory tracking of quadrotor UAVs," *Nonlinear Dyn.*, vol. 97, no. 1, pp. 1–19, Jul. 2019.

[13] S. Bouabdallah, A. Noth, and R. Siegwart, "PID vs LQ control techniques applied to an indoor micro quadrotor," in *Proc. IEEE/RSJ Int. Conf. Intell. Robots Syst.*, vol. 3, Sendai, Japan, 2004, pp. 2451–2456.

[14] M. Idres, O. Mustapha, and M. Okasha, "Quadrotor trajectory tracking using PID cascade control," *IOP Conf. Ser. Mater. Sci. Eng.*, vol. 270, Dec. 2017, Art. no. 012010.

[15] F. Chen, R. Jiang, K. Zhang, B. Jiang, and G. Tao, "Robust backstepping sliding-mode control and observer-based fault estimation for a quadrotor UAV," *IEEE Trans. Ind. Electron.*, vol. 63, no. 8, pp. 5044–5056, Aug. 2016.

[16] G. Sun and Z. Ma, "Practical tracking control of linear motor with adaptive fractional order terminal sliding mode control," *IEEE/ASME Trans. Mechatronics*, vol. 22, no. 6, pp. 2643–2653, Dec. 2017.

[17] X. Shi, Y. Cheng, C. Yin, S. Zhong, X. Huang, K. Chen, and G. Qiu, "Adaptive fractional-order SMC controller design for unmanned quadrotor helicopter under actuator fault and disturbances," *IEEE Access*, vol. 8, pp. 103792–103802, May 2020.

[18] Y. Yang and Y. Yan, "Attitude regulation for unmanned quadrotors using adaptive fuzzy gain-scheduling sliding mode control," *Aerosp. Sci. Technol.*, vol. 54, pp. 208–217, Jul. 2016.

[19] H. Du, X. Yu, M. Z. Q. Chen, and S. Li, "Chattering-free discrete-time sliding mode control," *Automatica*, vol. 68, pp. 87–91, Jun. 2016.

[20] J.-J. Xiong and G.-B. Zhang, "Global fast dynamic terminal sliding mode control for a quadrotor UAV," *ISA Trans.*, vol. 66, pp. 233–240, Jan. 2017.

[21] Y. Chen, W. Zhan, B. He, L. Lin, Z. Miao, X. Yuan, and Y. Wang, "Robust control for unmanned aerial manipulator under disturbances," *IEEE Access*, vol. 8, pp. 129869–129877, Jul. 2020.

[22] S. Park, H. Lee, S. Han, and J. Lee, "Adaptive fuzzy super-twisting backstepping control design for MIMO nonlinear strict feedback systems," *Int. J. Control, Autom. Syst.*, vol. 16, no. 3, pp. 1165–1178, Apr. 2018.

[23] F. Muñoz, I. González-Hernández, S. Salazar, E. S. Espinoza, and R. Lozano, "Second order sliding mode controllers for altitude control of a quadrotor UAS: Real-time implementation in outdoor environments," *Neurocomputing*, vol. 233, pp. 61–71, Apr. 2017.

[24] J. A. Moreno and M. Osorio, "Strict Lyapunov functions for the super-twisting algorithm," *IEEE Trans. Autom. Control*, vol. 57, no. 4, pp. 1035–1040, Apr. 2012.

[25] S. Mondal and C. Mahanta, "A fast converging robust controller using adaptive second order sliding mode," *ISA Trans.*, vol. 51, no. 6, pp. 713–721, Nov. 2012.

[26] S. Ding, J. Wang, and W. X. Zheng, "Second-order sliding mode control for nonlinear uncertain systems bounded by positive functions," *IEEE Trans. Ind. Electron.*, vol. 62, no. 9, pp. 5899–5909, Sep. 2015.

[27] A. Aboudonia, R. Rashad, and A. El-Badawy, "Composite hierarchical anti-disturbance control of a quadrotor UAV in the presence of matched and mismatched disturbances," *J. Intell. Robotic Syst.*, vol. 90, nos. 1–2, pp. 201–216, Sep. 2017.

[28] O. Mofid and S. Mobayen, "Adaptive sliding mode control for finite-time stability of quad-rotor UAVs with parametric uncertainties," *ISA Trans.*, vol. 72, pp. 1–14, Jan. 2018.

[29] C. Deng and G.-H. Yang, "Distributed adaptive fault-tolerant control approach to cooperative output regulation for linear multi-agent systems," *Automatica*, vol. 103, pp. 62–68, May 2019.
[30] L. Zhang, Y. Li, and S. Tong, "Adaptive fuzzy output feedback control for MIMO switched nonlinear systems with prescribed performances," *Fuzzy Sets Syst.*, vol. 306, pp. 153–168, Jan. 2017.
[31] S. Li, Y. Wang, J. Tan, and Y. Zheng, "Adaptive RBFNNs/integral sliding mode control for a quadrotor aircraft," *Neurocomputing*, vol. 216, pp. 126–134, Dec. 2016.
[32] J. Park and I. W. Sandberg, "Universal approximation using radial-basis-function networks," *Neural Comput.*, vol. 3, no. 2, pp. 246–257, Jun. 1991.
[33] C. Xi, D. Zhai, J. Dong, and Q. Zhang, "Approximationbased adaptive fuzzy tracking control for a class of switched nonlinear pure-feedback systems," *Int. J. Syst. Sci.*, vol. 48, no. 12, pp. 2463–2472, May 2017.
[34] Y. Zhang, Z. Chen, M. Sun, and X. Zhang, "Trajectory tracking control of a quadrotor UAV based on sliding mode active disturbance rejection control," *Nonlinear Anal. Model. Control*, vol. 24, no. 4, pp. 545–560, Jun. 2019.
[35] Z. Li, X. Ma, and Y. Li, "Robust trajectory tracking control for a quadrotor subject to disturbances and model uncertainties," *Int. J. Syst. Sci.*, vol. 51, no. 5, pp. 839–851, Apr. 2020.
[36] K. Sasaki and Z.-J. Yang, "Disturbance observer-based control of UAVs with prescribed performance," *Int. J. Syst. Sci.*, vol. 51, no. 5, pp. 939–957, Apr. 2020.
[37] M. Labbadi and M. Cherkaoui, "Robust adaptive nonsingular fast terminal sliding-mode tracking control for an uncertain quadrotor UAV subjected to disturbances," *ISA Trans.*, vol. 99, pp. 290–304, Apr. 2020.
[38] J. A. Moreno and M. Osorio, "A Lyapunov approach to second-order sliding mode controllers and observers," in *Proc. 47th IEEE Conf. Decis. Control*, Dec. 2008, pp. 2856–2861.
[39] Y. Wang, B. Jiang, Z.-G. Wu, S. Xie, and Y. Peng, "Adaptive sliding mode fault-tolerant fuzzy tracking control with application to unmanned marine vehicles," *IEEE Trans. Syst., Man, Cybern. Syst.*, early access, Jan. 24, 2020, doi: 10.1109/TSMC.2020.2964808.
[40] S. Xiao and J. Dong, "Robust adaptive fault-tolerant control for time delay uncertain nonlinear systems with time-varying performance bounds," *Int. J. Syst. Sci.*, vol. 50, no. 11, pp. 2168–2188, Aug. 2019.
[41] E.-H. Zheng, J.-J. Xiong, and J.-L. Luo, "Second order sliding mode control for a quadrotor UAV," *ISA Trans.*, vol. 53, no. 4, pp. 1350–1356, Jul. 2014.
[42] C. Kang, S. Wang, W. Ren, Y. Lu, and B. Wang, "Optimization design and application of active disturbance rejection controller based on intelligent algorithm," *IEEE Access*, vol. 7, pp. 59862–59870, 2019.
[43] P. Du, J. Huang, D. Wu, and F. Ding, "PSO-optimized fuzzy control for four-rotor unmanned aerial vehicle with suspended load," in *Proc. IEEE 8th Annu. Int. Conf. Cyber Technol. Autom., Control, Intell. Syst. (CYBER)*, Jul. 2018, pp. 474–479.
[44] Z. L. Ma, H. X. Li, Y. M. Gu, Z. Y. Li, and Q. Q. Li, "Flight and hover control system design for a mini-quadrotor based on multi-sensors," *Int. J. Control Autom. Syst.*, vol. 17, no. 2, pp. 486–499, Jan. 2019.
[45] B. Xiao, Q. Hu, and Y. Zhang, "Fault-tolerant attitude control for flexible spacecraft without angular velocity magnitude measurement," *J. Guid., Control, Dyn.*, vol. 34, no. 5, pp. 1556–1561, Sep. 2011.

BOWEN XU received the B.E. degree in industrial engineering and the M.E. degree in mechanical engineering from the College of Mechanical and Vehicle Engineering, Hunan University, Changsha, China, in 2013 and 2016, respectively. He is currently pursuing the Ph.D. degree with the School of Mechanical and Electrical Engineering, Central South University, Changsha. His research interests include nonlinear system modeling, control engineering, and industrial engineering.

XINJIANG LU (Member, IEEE) received the B.E. and M.E. degrees from the School of Mechanical and Electrical Engineering, Central South University, China, and the Ph.D. degree from the Department of Manufacturing Engineering and Engineering Management, City University of Hong Kong, Hong Kong. He is currently a Professor with the School of Mechanical and Electrical Engineering, Central South University. His research interests include machine learning, process modeling and control, and integration of design and control. He received the Excellent Thesis Award for the master's degree, Hunan, in 2007, the Hiwin Doctoral Dissertation Award, in 2011, the New Century Excellent Talents Award from the Chinese Ministry of Education, in 2013, and the Hunan Provincial Science Fund for Distinguished Young Scholars, in 2019. He served on editorial board membership of three international journals.